Molecular simulation of nano-dispersed fluid phases

Martin Horsch*, Hans Hasse

Lehrstuhl für Thermodynamik, Technische Universität Kaiserslautern, Erwin-Schrödinger Str. 44, 67663 Kaiserslautern, Germany

Abstract

Fluid phase equilibria involving nano-dispersed phases, where at least one of the coexisting phases is confined to a small volume, are investigated by molecular dynamics simulation. Complementing previous studies on nanoscopic droplets, simulation volumes containing a nanoscopic gas bubble surrounded by a subsaturated liquid phase under tension, i.e. at negative pressure, are conducted in the canonical ensemble. The boundary conditions are chosen such that the phase equilibrium at the curved interface is thermodynamically stable. Two distinct size-dependent effects of opposite sign are found for the density of the gas in the centre of the bubble. The curvature dependence of the surface tension is considered, employing an approach based directly on the average radial density profiles.

Keywords: Phase equilibria, Bubble, Metastable liquid, Simulation, Interfacial tension, Nanostructure

*Corresponding author. E-mail: martin.horsch@mv.uni-kl.de; phone: +49 631 205 3227; fax: +49 631 205 3835.

1. Introduction

Dispersed phases are ubiquitous both in nature and technological applications. Their character poses a particular challenge to thermodynamic approaches which attempt to reduce the complexity of a system to a few macroscopic degrees of freedom. Even in the most bulk-like central region of a nanoscopic bubble or droplet, thermodynamic properties may deviate substantially from the bulk phase under corresponding conditions. Interfacial properties may dominate, and the heterogeneity of the dispersion further complicates its thermodynamic description.

Phenomenological thermodynamics was applied to fluid interfaces by Gibbs [1], whose approach ultimately succeeded due to the rigour with which it unifies the macroscopic and microscopic points of view. In particular, it reduces the phase boundary, which is continuous on the molecular level, to a strictly two-dimensional dividing surface separating two bulk phases. The deviation between the actual system and the theoretical system, consisting of the two bulk phases only, serves as a definition of interfacial excess quantities to which phenomenological thermodynamic reasoning can be applied.

This reduction facilitates discussing and analysing systems which contain a nano-dispersed phase, but it does so at a prize. The task of representing physically complex behaviour is shifted to the interfacial excess quantities. Such quantities, and particularly the surface tension and the adsorption, have to account for all the aspects which distinguish, for instance, the bulk metal from a metal nanoparticle, or the bulk vapour from a gas bubble that contains a few molecules only. This explains why such fundamental and apparently simple issues such as the dependence of the surface tension of small gas

bubbles and liquid droplets on their radius are still not fully settled, despite having been on the agenda of scientific discussions for decades.

Furthermore, for the development of molecular equations of state [2–4], which mostly aim at describing the bulk phases, it is important to understand how precisely the intermolecular interactions affect the association of molecules to small nanoclusters, since the underlying thermodynamic perturbation theory [5, 6] is based on a statistical-mechanical cluster expansion [7]. In addition, a reliable description of natural phenomena such as atmospheric nucleation, as well as engineering problems such as nucleate pool boiling, spray cooling, or nucleation in expanding gases as it is ubiquitous in turbines, can only be obtained on the basis of quantitatively accurate models for the thermodynamic properties of the respective dispersed fluid phases, i.e. nanoscopic gas bubbles and liquid droplets. For such studies, both static and dynamic properties have to be captured, concerning physical objects which can fluctuate significantly in their size and shape or even disappear in the blink of an eye.

It is therefore attractive to apply molecular simulation to study these problems, supplementing experimental results where they are available, and replacing them where suitable experiments have not yet been devised. Molecular dynamics (MD) simulation is capable of elucidating the properties of nano-dispersed phases in equilibrium [8–10] as well as dynamic phenomena including nucleation [10, 11], aggregation [12], coalescence [13], growth [14], and dynamic wetting [15], among many others [16, 17], at molecular resolution. Even complex scenarios, such as gold clusters with an organic protection layer, are well accessible to MD simulation [18]. In a simulation, boundary

conditions can be imposed which would be hard or impossible to guarantee in an experimental setting. For instance, transport processes can be sampled in a well-defined steady state by non-equilibrium MD simulation, including the coupled heat and mass transfer occurring at interfaces [16] and during nucleation in a supersaturated vapour [11]. The critical nucleus of a nucleation process, which corresponds to a free energy maximum and is therefore thermodynamically unstable, can be investigated in detail by equilibrium simulation of a small system in the canonical ensemble [10].

As a massively-parallel high performance computing application, MD simulation scales well both in theory and in practice. Up to trillions of interaction sites can be simulated [19], so that a single modelling approach can be employed from the nanometre up to the micrometre length scale. As such, molecular simulation is a useful tool for investigating the size dependence of interfacial effects. MD simulations of the surface tension of curved vapour-liquid interfaces, comparing it with that of the planar phase boundary, were already conducted in the 1970s [8]. Many of the subsequent contributions to this problem, in particular more recently, have been guided by the analysis of molecular simulation results [9, 10, 20–27].

The present work illustrates the contribution that molecular modelling and simulation can make to the discussion of nano-dispersed phases, with a focus on MD simulation of a gas bubble in equilibrium with a liquid at negative pressure. This case is both of fundamental scientific interest and technically important, e.g. for cavitation. In Section 2, a brief survey is given on the relevant aspects of the theory of vapour-liquid interfaces, including the dependence of the surface tension on curvature and its relation to the excess

equimolar radius; for an introduction to dispersed phase thermodynamics from a more general point of view, the interested reader is referred to the books by Hill [28], Kashchiev [29], Rowlinson and Widom [30], as well as Vehkamäki [31]. Section 3 introduces the employed molecular simulation methods. Simulation results, consistently finding the excess equimolar radius to be positive, are presented in Section 4. A possible interpretation of the present results is suggested in Section 5, relating it to previous work and leading to the conclusion which is given in Section 6.

2. Thermodynamics of dispersed phases

2.1. Vapour-liquid surface tension

The tension of a planar fluid interface can be defined in different ways, following a thermodynamic or a mechanical approach. Thermodynamically, the surface tension γ can be expressed by the partial derivative of the free energy A over the surface area F at constant number of molecules $\mathbf{N}$ (of all components), volume V, and temperature T:

$$\gamma = \left(\frac{\partial A}{\partial F} \right)_{\mathbf{N},V,T} . \tag{1}$$

The surface free energy can then be obtained by integration

$$A_F = \int_0^F \gamma \, dF, \tag{2}$$

over a process during which the interface is created.

By molecular simulation, the thermodynamic surface tension can be computed from the test area method [32], while grand canonical Monte Carlo simulation can be employed to obtain A_F from the excess Landau free energy corresponding to the respective density [20, 33].

Neglecting size effects on γ, the surface free energy can be approximated by $A_F \approx \gamma F$. While such a simplification is justified for macroscopic systems, it may violate the thermodynamics of small systems [28], where, in general, significant finite size effects can be present even for planar phase boundaries [34, 35].

For a mechanical definition, the surface tension is treated as causing a force f_τ acting in tangential direction (with respect to the interface), i.e. a tendency of the interface to contract. The mechanical surface tension

$$\gamma = \frac{f_\tau}{l} \tag{3}$$

relates the magnitude of this force to the length of the contact line l between the interface and the surface of another mechanical object, e.g. a confining wall, on which the force f_τ acts.

In a cuboid box with the extension $V = l_x \times l_y \times l_z$, which contains a planar interface normal to the z axis, the interface and the two faces of the box which are normal to the x axis have contact lines with an elongation of l_y, cf. Fig. 1. Each of these faces (normal to x) has an area of $F_{yz} = l_y \times l_z$. The tangential force $f_\tau = f_x = \gamma l_y$ thus constitutes a negative (contracting) contribution to the pressure, acting in tangential direction, i.e. in x-direction here.

The surface tension can thus be obtained from the deviation between the tangential and normal eigenvalues p_τ and p_ν of the pressure tensor:

$$p_\tau - p_\nu = -\frac{\gamma l_y}{F_{yz}} = -\frac{\gamma}{l_z}. \tag{4}$$

In the example discussed above, the tangential pressure $p_\tau = p_x = p_y$ acts in the x- and y-directions parallel to the interface, while the normal pressure

acts in z-direction perpendicular to the interface. It is well known that for planar fluid phase boundaries, the thermodynamic and mechanical definitions of γ coincide [36]. In molecular simulation, where the pressure tensor is computed from the virial, an approach referred to as the virial route relies on Eq. (4) to obtain the surface tension [9, 37].

2.2. Curved vapour-liquid interfaces

At the curved interface of a bubble or a droplet, the mechanical equilibrium condition is characterized by the Laplace equation

$$\Delta p = p' - p'' = \frac{2\gamma}{R}, \tag{5}$$

where p' and p'' denote the pressure in the liquid and the vapour phase, respectively. The radius R for which this relation holds is called the Laplace radius or the radius of the surface of tension. The interface tends to contract, compressing the dispersed phase which is situated inside, and the surface tension γ couples this compressing effect with its cause, the curvature of the interface. By convention, the radius R is positive in case of a droplet (with $p' > p''$) and negative in case of a bubble (with $p' < p''$).

It is worth recalling that within the thermodynamic approach of Gibbs [1], the position of the formal dividing surface is arbitrary at first. Thus, a further condition, such as Eq. (5), is needed to define a radius. The values of p' and p'' do not necessarily agree with the actual mechanical pressures on the two sides of the interface. They are obtained by combining the mechanical equilibrium condition, Eq. (5), with the chemical and thermal equilibrium conditions, i.e. equal chemical potential ${\mu_i}' = {\mu_i}''$ for all components i and

equal temperature $T' = T''$. The relation between the values of μ_i, p, and T is given by the equation of state for the bulk phases.

For the case of a pure fluid below the critical temperature, a $\mu - p$ diagram [38] visualizes the impact of curvature, by means of a vapour-liquid equilibrium condition with a pressure difference between both phases, as expressed by Eq. (5), on other thermodynamic properties such as the density of the coexisting fluid phases and the chemical potential, cf. Fig. 2. The residual chemical potential μ_{res} is defined by the deviation of the chemical potential μ from its ideal temperature-dependent (i.e. density-independent) contribution μ_{id}, reduced by temperature [39]

$$\mu_{\mathrm{res}}(\rho, T) = \frac{\mu(\rho, T) - \mu_{\mathrm{id}}(T)}{T}. \tag{6}$$

At low densities it can be approximated by $\mu_{\mathrm{res}} \approx \ln \rho$, so that the vapour parts of the three isotherms shown in Fig. 2 coincide roughly. Its derivative with respect to pressure at constant temperature is given by

$$\left(\frac{\mu_{\mathrm{res}}}{p}\right)_T = \frac{1}{\rho T}. \tag{7}$$

Hence, proceeding (at increasing ρ) from stable vapour to metastable vapour, to the unstable part of the isotherm, the metastable and finally the stable liquid, the slope of the curves in the $\mu - p$ diagram decreases successively. In Fig. 2 it can be seen how $\Delta p = p' - p'' > 0$, corresponding to a droplet, induces a vapour-liquid equilibrium at a supersaturated chemical potential with $\mu > \mu_{\mathrm{sat}}$, where μ_{sat} is the chemical potential for the equilibrium at a planar interface. Obversely, in case of a bubble, the pressure is higher in the gas phase, i.e. $\Delta p < 0$, so that the coexisting phases become subsaturated ($\mu < \mu_{\mathrm{sat}}$).

While the thermodynamic and the mechanical approaches to defining the surface tension, see Eqs. (1) and (3), respectively, are strictly equivalent for planar fluid interfaces, cf. Section 2.1, this is not the case for solid systems, where the pressure tensor in the bulk is not necessarily isotropic [40]. Also for nano-dispersed fluid phases, where an isotropic bulk-like region may be completely absent, thermodynamic and mechanical definitions of γ deviate from each other [26, 27]: Mechanical approaches following the virial route have found the surface tension of nanodroplets to be significantly smaller than that of the planar vapour-liquid interface [9, 41], whereas the thermodynamic routes, i.e. the test area method [23] and grand canonical Monte Carlo simulation [22], do not confirm this and find such an effect to be much weaker or even of opposite sign.

An explanation of this disagreement between mechanical and thermodynamic expressions for the surface tension is possibly to be found in the observation of Percus et al. [42] that in general, the Landau free energy deviates from the volume integral over the local pressure for inhomogeneous fluid systems. In any case, it is clear that the quantity which is relevant to the Gibbs approach is the thermodynamic surface tension and not the mechanical one.

Properties related to the smallest clusters, i.e. dimers, trimers, etc., which are always present in a stable vapour, can in principle be determined by an exact statistical-mechanical approach based on the cluster expansions of Mayer [7], Born and Fuchs [43]. As mentioned above, the modern molecular equations of state from the SAFT [2] and BACKONE [3] families are based on this approach. With some effort (which would involve developing a

suitable concept of association), a molecular equation of state could possibly be employed to compute quantities such as the monomer fraction as well as higher-order cluster properties. In the literature, it has already been attempted to extrapolate from the dimer fraction in a stable vapour, obtained from the second virial coefficient, to the number of larger liquid nuclei formed in a supersaturated vapour [44, 45].

While it is relatively uncommon to extrapolate from small clusters to larger ones, an obverse approach which extrapolates from small (or zero) to high curvature, is very widespread. The characteristic length scale for the dependence of the surface tension on the radius is the Tolman length

$$\delta = R_\rho - R, \tag{8}$$

introduced by Tolman [46, 47] who applied the theoretical framework of Gibbs [1] to the adsorption Γ, i.e. the excess density, at the spherical surface corresponding to the Laplace radius R. The Tolman length expresses the deviation of the equimolar radius R_ρ, which corresponds to the spherical dividing surface with zero adsorption, from the Laplace radius R. It determines the dependence of the surface tension on curvature according to the thermodynamically exact, non-truncated version of the Tolman equation [47]

$$\frac{1}{\gamma}\frac{d\gamma}{dR} = \frac{[2\delta/R^2]\,[1 + (\delta/R) + (\delta^2/3R^2)]}{1 \,+\, [2\delta/R]\,[1 + (\delta/R) + (\delta^2/3R^2)]}, \tag{9}$$

which, by straightforward algebraic manipulation, transforms to [26]

$$\frac{d\ln R}{d\ln \gamma} = 1 + \frac{1}{2}\left(\frac{\delta}{R} + \left[\frac{\delta}{R}\right]^2 + \frac{1}{3}\left[\frac{\delta}{R}\right]^3\right)^{-1}. \tag{10}$$

Although Tolman [47] conjectured δ to be positive and its dependence on the radius to be of secondary importance, Eq. (10) is valid for any magnitude and

dependence on R of the Tolman length. However, its common interpretation as an expansion in terms of $1/R$, i.e.

$$\frac{\gamma}{\gamma_\parallel} = \frac{1}{1 + 2\delta_\parallel R^{-1} + \ldots}, \tag{11}$$

has more recently come under criticism for a variety of reasons [20, 25], discussed here in Sections 5 and 6. In any case, Eq. (11) has the advantage of being based directly on the Tolman length $\delta_\parallel$ and the surface tension $\gamma_\parallel$ of the planar vapour-liquid interface which can be investigated experimentally in a stable state, as opposed to nano-dispersed phases where this is in most cases practically impossible.

The Laplace radius R has the disadvantage of being defined by the surface tension of the curved interface, which is thermodynamically well-defined, but hard to determine. In consequence, it is often impossible to tell how many molecules are inside a bubble or a droplet with the Laplace radius R (which would be precisely known if an equimolar radius was specified), or which chemical potential and pressure difference correspond to a particular value of R. Hence, considering that the dependence of the surface tension on curvature is under dispute at present, Eq. (5) contains two unknowns and the Laplace radius is ill-defined at first.

For this reason, direct routes to the Tolman length have been proposed which effectively eliminate the Laplace radius [48–51]. The approach of Nijmeijer et al. [48] as well as van Giessen and Blokhuis [50] can be formulated in terms of the equimolar surface tension, defined here by

$$\gamma_\rho = \frac{R_\rho(p' - p'')}{2} = \frac{\gamma R_\rho}{R}, \tag{12}$$

and its relation to the equimolar curvature $1/R_\rho$. In the planar limit, i.e.

$1/R_\rho \to 0$, the equimolar surface tension approaches the surface tension of the planar vapour-liquid interface

$$\lim_{1/R_\rho \to 0} \gamma_\rho = \left(\lim_{1/R_\rho \to 0} \gamma \right) \cdot \left(\lim_{1/R_\rho \to 0} \frac{R_\rho}{R} \right) = \gamma_\parallel. \tag{13}$$

An analogous relation holds for the derivative of the surface tension with respect to curvature [26, 48]

$$\begin{aligned} \lim_{1/R_\rho \to 0} \left(\frac{\partial \gamma_\rho}{\partial (1/R_\rho)} \right)_T &= \lim_{1/R_\rho \to 0} \left(\frac{\partial \gamma}{\partial (1/R)} \right)_T \\ &= -2\delta_\parallel \gamma_\parallel, \end{aligned} \tag{14}$$

relating it to the Tolman length in the planar limit.

If the surface tension of the planar interface, rather than the actual surface tension of the curved interface, is inserted into the Laplace equation

$$\Delta p = p' - p'' = \frac{2\gamma_\parallel}{R_\kappa}, \tag{15}$$

a direct route to δ can be also be expressed in terms of the capillarity radius R_κ, defined by Eq. (15). In this reformulation of Tolman's theory, Eqs. (8) – (11) transform to [26]

$$\eta = R_\rho - R_\kappa, \tag{16}$$

$$\frac{d \ln \gamma}{d \ln(\gamma_\parallel / R_\kappa)} = \frac{2}{3} \left(1 - \left[\frac{\gamma_\parallel (1 + \eta R_\kappa^{-1})}{\gamma} \right]^3 \right), \tag{17}$$

$$\frac{\gamma}{\gamma_\parallel} = 1 + 2\frac{\eta_\parallel}{R_\kappa} - 2\left(\frac{\eta_\parallel}{R_\kappa} \right)^2 + \ldots, \tag{18}$$

wherein η is referred to as the excess equimolar radius. It should be noted that in the planar limit, the Tolman length and the excess equimolar radius are of the same magnitude, but of opposite sign [26]

$$\delta_\parallel = -\eta_\parallel, \tag{19}$$

despite their similar definition.

In previous work following the approach described above, only the case of a liquid droplet surrounded by gas has been considered [26]. In the present work, it is applied to MD simulation results for simulation volumes containing a gas bubble surrounded by a subsaturated liquid phase, cf. Section 4. For such systems, equimolar radii R_ρ and capillarity radii R_κ are determined here from average radial density profiles, and the equimolar surface tension γ_ρ is computed.

3. Molecular simulation methodology

3.1. Simulation software and molecular model

The present work applies MD simulation to the problems outlined above. For this purpose, we employed the program *ls1 mardyn* [52], i.e. '**l**arge **s**ystems **1**st by **m**olecu**lar dyn**amics'. Eckhardt et al. [19] have recently observed that *ls1 mardyn* scales well in its parallelized mode, delivering an almost ideal speedup on modern supercomputer architectures and even achieving a world record in system size for molecular simulation, with $N > 4 \times 10^{12}$. The scenarios considered here are smaller by far, but partly require a long simulation time, so that an efficient simulation code was a prerequisite for carrying out the present study as well.

Since the theoretical state of the art leaves many qualitative problems open for an investigation on the molecular level, the Lennard-Jones truncated-shifted (LJTS) pair potential was selected as the molecular model under consideration here. In reduced units, i.e. setting the Lennard-Jones size and energy parameters $\sigma = 1$ and $\epsilon = 1$ (as well as the Boltzmann constant

$k = 1$) to unity, it is given by

$$u(r) = \begin{cases} 4\left[(r^{-12} - r^{-6}) - (r_\mathrm{c}^{-12} - r_\mathrm{c}^{-6})\right], & r < r_\mathrm{c}, \\ 0, & r \geq r_\mathrm{c}, \end{cases} \tag{20}$$

where r is the distance between two molecules and $r_\mathrm{c} = 2.5$ is the cutoff radius. Since the LJTS pair potential is a quantitatively precise model for methane and several noble gases, including their vapour-liquid surface tension [9], the present results also can be given a realistic interpretation.

This choice of molecular model was also driven by the fact that vapour-liquid interfacial properties of the LJTS fluid have been addressed in previous work from several groups [9, 24, 41, 48, 50], employing different methods which can thus be compared directly. The truncated-shifted cutoff, cf. Eq. (20), is continuous in terms of the potential, but not with respect to the force which has a discontinuity at $r = r_\mathrm{c}$. The intermolecular interaction is thereby strictly limited to radii smaller than r_c, avoiding the complex issue of long-range cutoff corrections in inhomogeneous systems [35, 53, 54].

3.2. Influence of curvature on vapour-liquid equilibria

Extending previous work on the excess equimolar radius of liquid droplets [26], a series of MD simulations was conducted for volumes containing a LJTS gas bubble in equilibrium with a subsaturated liquid. The simulations were carried out in the canonical ensemble with a periodic boundary condition. The initial conditions were chosen such that one single bubble existed in the centre of the simulation box. The size of that bubble was controlled by choosing the number of molecules and the simulation volume appropriately. As pointed out by Fisher and Wortis [55] as well as Reguera et al. [56],

such equilibria can be thermodynamically stable, even if the phase (here, the liquid) which surrounds the dispersed phase (here, the gas bubble) would be metastable in a corresponding homogeneous state. In such a case, the simulation volume has to be relatively small – the precise conditions depend on the equation of state of the fluid – for configurations containing a single gas bubble.

The present MD simulations are therefore concerned with the scenario where a single gas bubble is surrounded by a subsaturated liquid phase, under equilibrium conditions for the pure LJTS fluid. To evaluate the equations of motion numerically, a Verlet leapfrog integrator was used, with an integration time step of 0.003 in reduced units. The total momentum of the system was neutralized every 16 000 time steps, by subtracting equal fractions of it from all molecules, and the system of coordinates was continuously shifted, following the random motion of the bubble to keep its centre in the origin. The temperature was specified to be $T = 0.75$, i.e. about 70 % of the critical temperature [9], and controlled by a velocity rescaling thermostat (also known as an isokinetic thermostat). A novel shading approach for the visualization of point-based datasets, which makes it easier to analyze the morphology of an interface on the molecular level [57], was applied to individual configurations, cf. Fig. 3.

The number of molecules N and the simulation volume $V = l \times l \times l$ were varied as indicated in Table 1. An equilibration was conducted for at least 400 000 time steps. Subsequently, density profiles were determined by binning over several averaging intervals of at least 200 000 time steps until the profiles of were found to converge. In one of the cases (with $N = 20$

514 and $V = 29\ 791$), bubble configurations were found to alternate with homogeneous subsaturated liquid configurations, cf. Fig. 4. This simulation was also evaluated, however, taking only such density profiles into account where a bubble was actually present.

From these density profiles, cf. Figs. 4 and 5, all quantities were determined which are relevant to the theoretical approach introduced in previous work [26] and discussed in Section 2.2. For this purpose, an extrapolated liquid density ρ'_∞ was determined from the limit to which the expression [26]

$$\rho_{\mathrm{corr}}(r) = \rho'_\infty - a' \exp\left(b' - c'r\right), \tag{21}$$

adjusted to the outer part of the density profile $\rho(r)$, in terms of the distance r from the centre of the bubble, converges at $r \to \infty$. Standard deviations on the basis of different density profiles, collected from the same simulation during successive time intervals, were calculated to estimate the simulation error. An analogous term [26]

$$\rho_{\mathrm{corr}}(r) = \rho''_{-\infty} + a'' \exp\left(b'' + c''r\right), \tag{22}$$

was adjusted to the inner part of the density profile. The criterion

$$\int_0^{R_\rho} dr\, r^2 \left[\rho(r) - \rho''_{-\infty}\right] + \int_{R_\rho}^{l/2} dr\, r^2 \left[\rho(r) - \rho'_\infty\right] \tag{23}$$

was then applied to the density profile, i.e. to the actual profile $\rho(r)$, not the correlation, to obtain the equimolar radius R_ρ [26].

However, in contrast with the method previously established for the simulation of liquid drops [26], the pressure p'' inside the gas bubble, and thereby the capillarity radius

$$R_\kappa = \frac{2\gamma_\parallel}{p' - p''}, \tag{24}$$

was not determined here from the density profile on the vapour side. Instead, exploiting the fact that the liquid phase can very accurately be sampled here, the extrapolated density ρ'_∞ of the subsaturated liquid surrounding the bubble was considered. It should be recalled that the values of p' and p'' which the theory requires are not the actual mechanical pressures outside and inside, but those of the respective subsaturated bulk phases at the same chemical potential (cf. the discussion in Section 2.2).

Therefore, the pressure of the vapour phase was determined here, accordingly, from the thermal and chemical equilibrium condition by means of an empirical fifth order virial equation of state [58]. For the subsequent discussion, however, this methodical issue is of minor importance: The pressure difference Δp, which yields the capillarity radius as defined by Eq. (15), is dominated by the contribution from the liquid phase, which was considered here by the same extrapolation method as previously published [26]. The surface tension of the planar vapour-liquid interface, which is needed to evaluate Eq. (15), was taken from Vrabec et al. [9]. The employed equation of state has been shown to agree with molecular simulation results on pressure, volume, and temperature for the LJTS fluid with a high degree of accuracy, particularly concerning metastable supersaturated vapours and subsaturated liquids [58].

In a second series of simulations, the qualitative influence of curvature was considered. For this purpose, canonical ensemble MD simulations were carried out for a bubble (surrounded by a subsaturated liquid), a droplet (surrounded by a supersaturated vapour), and a system consisting of a vapour and a liquid slab separated by planar interfaces. For these systems, the chem-

ical potential was computed by applying the Widom test particle method [59] with N test insertions and deletions every 16 time steps, where N is the number of particles in the system. To compensate for the additional computational effort, the averaging interval for constructing the profiles was reduced to 10 000 time steps here.

The simulation conditions were chosen here such that the radii of the droplet and the bubble were about 8.5, while the thickness of the vapour and the liquid slab was about 12.5, complementing previous simulation results [60]. The subsaturation (for bubbles) or supersaturation (for droplets) was determined from the deviation

$$\Delta\mu = \mu - \mu_{\mathrm{sat}} \tag{25}$$

between the chemical potential in the system with the curved interface and the value μ_{sat} computed at the planar interface. On this basis, p' as well as p'' for the second series of simulations were calculated from the virial equation for the LJTS fluid [58].

4. Simulation results

The density profiles of gas bubbles in equilibrium with subsaturated liquid phases, which were obtained by MD simulation in the canonical ensemble, are shown in Fig. 5. The density in the centre of the bubble should be expected to approach the saturated vapour density, i.e. $\rho''(T = 0.75) = 0.0124$ [9], in the limit of an infinitely large bubble ($R \to -\infty$), which corresponds to the transition to a planar interface. The present simulation results confirm this, cf. Tab. 1 and the results for $R_\rho = -28$ shown therein. Moreover, deviations

of the vapour density from its value at saturation over a planar interface ρ''_{sat} are observed for small bubbles, cf. Fig. 6. This deviation is caused by two qualitatively distinct effects:

1. For relatively large bubbles ($-\infty < R_\rho < -9$), the density in the centre decreases as the size of the bubble becomes smaller. The minimal gas density observed in the present series of simulations, which is significantly below 0.01, is found in the centre of the bubble with $R_\rho = -8.7$.
2. For even smaller bubbles ($-9 < R_\rho < 0$), the density in the centre increases again. In the smallest case considered here, i.e. $R_\rho = -5.6$, the gas phase is found to be much denser than that which coexists with the liquid at a planar interface, cf. Fig. 5.

In Tab. 1, numerical results are shown that were obtained from these simulations by following the approach outlined in Section 3.2, based on liquid densities extracted from the present density profiles.

To assess the viability of the approach [26], the maximal density ρ'_{max}, i.e. the density reached at the outer end of the simulation box, is compared with the extrapolated liquid density ρ'_∞ in Tab. 1. In case of a very small volume available for the liquid, there could be a significant deviation between these two densities due to the absence of a sufficiently bulk-like region in the liquid phase. For the present series of simulations, however, the extrapolated and maximal densities are virtually identical, even for the smallest bubbles.

To illustrate the influence of the interfacial curvature, the density of the liquid surrounding the bubbles is contrasted in Fig. 7 with the saturated bulk liquid density, as given by the correlation of Vrabec et al. [9]. This correlation has a standard deviation of $\delta\rho'_{\mathrm{corr}} = 0.0001$ from the outcome of six Grand

Equilibrium simulations in the temperature range $0.67 \leq T \leq 0.82$ with a simulation uncertainty of $\delta\rho'_{\mathrm{sim}} \leq 0.0002$ [9]. The bubble density of the bulk LJTS fluid at $T = 0.75$ is thereby given as $\rho'_{\mathrm{sat}} = 0.7594 \pm 0.0003$.

The density of the liquid phase surrounding the gas bubble was found to be significantly subsaturated, since the deviation between ρ'_{sat} and ρ'_{∞} is over four times larger than the accumulated error for both quantities in all cases. In particular, as shown in Fig. 7, smaller bubbles consistently correspond to smaller liquid densities here, in agreement with capillary theory. The excess equimolar radius $\eta = R_\rho - R_\kappa$ was found to be positive, indicating a deviation from the capillarity approximation where, to first order in $1/R$, the surface tension of a droplet is larger and the surface tension of a bubble is smaller than that of the planar vapour-liquid interface.

Results for the chemical potential of bubbles, planar slabs, and droplets, cf. Tab. 2, corroborate the thermodynamic approach to the analysis of curved interfaces outlined in Section 2.2. The chemical potential of droplets (and the vapour surrounding them) was consistently found to be higher than the value at saturation over a planar interface. Obversely, nanoscopic gas bubbles and the liquid phase surrounding them are subsaturated, and the deviation from μ_{sat} increases as the dispersed phase becomes smaller.

5. Discussion

As pointed out above, it is one of the observations from the present simulations of curved vapour-liquid interfaces that a nanobubble with a diameter larger than 5 nm, roughly corresponding to $|R| > 6$ for the LJTS fluid [9], has a smaller density than the bulk vapour at the dew line (see Fig. 5). This

is the behaviour which should be expected from capillary theory, based on Gibbs' thermodynamic interpretation of the Laplace equation. It was also confirmed that the subsaturated density corresponds to a subsaturated chemical potential ($\mu < \mu_{\mathrm{sat}}$), cf. Tab. 2, in agreement with the thermodynamic discussion of the curvature influence on fluid phase coexistence (see Fig. 2).

On the other hand, the vapour density in the centre of the bubble was found to increase again for even smaller bubbles, eventually exceeding the dew density. This is not paralleled by an increase, but rather by a further decrease of the liquid density, cf. Fig. 7, which suggests that in terms of the chemical potential, these extremely small bubbles are subsaturated as well. This implies that among the two effects present for the gas density, only one affects the surrounding liquid as well, suggesting the following interpretation: Both phases, vapour and liquid, tend to become subsaturated due to *interfacial curvature*, cf. Fig. 2. The density in the centre of the bubble, however, experiences an additional obverse influence due to a size-dependent phenomenon which is distinct from curvature.

The density profiles, cf. Fig. 5, suggest that the density of the gas phase is increased *not due to curvature*, which tends to reduce μ and thereby also ρ'', but because there is not enough space available in radial direction for the density profile to converge to the bulk density that would correspond to the respective value of μ. Therefore, this second effect should be ascribed to the extremely *small diameter* of the nanobubbles. In the present simulations, however, no analogous effect is found in the liquid phase. This may be related to the fact that the liquid has a much higher density, so that a perturbation which is significant for ρ'' may well appear to be negligible in comparison

with ρ'.

This parallels the recent discovery, by Malijevský and Jackson [27], of two distinct size-dependent effects concerning the surface tension of nanodroplets: The Tolman length δ was found to be negative, causing the surface tension to increase over its planar value. The leading term, which dominates this effect for relatively large radii, is proportional to $1/R$. Extremely small droplets, however, exhibit a reduced surface tension. From an empirical correlation, Malijevský and Jackson [27] found this contribution to γ, which acts obversely to Tolman's curvature effect, to be proportional to $1/R^3$.

In a subsequent study of Werth et al. [35], the surface tension of thin planar liquid slabs with a thickness of s was found to be reduced, with respect to the macroscopic vapour-liquid surface tension, by a term proportional to $1/s^3$. Furthermore, density profiles revealed the density in the centre of these nanoslabs to deviate from the density of the saturated bulk liquid by a term proportional to $1/s^3$ as well, suggesting that the two phenomena are related expressions of a single effect which is caused by the small thickness of the interface [35].

The present results complement this picture. They support the hypothesis that for gas bubbles as well, there are distinct effects due to curvature on the one hand and due to the small diameter on the other hand, cf. Fig. 6. This corroborates the analysis of Malijevský and Jackson [27]. For the surface tension of a bubble, however, these two effects do not counteract but rather reinforce each other, since both the curvature effect from the Tolman equation (with $\delta < 0$ [27] and a negative curvature) and the small-diameter effect contribute to a reduction of γ.

This is confirmed by an analysis following the approach of Nijmeijer et al. [48] as well as van Giessen and Blokhuis [50], applied to the previous simulations of single droplets [26] and the present simulations of single bubbles, cf. Tab. 3. In particular, the equimolar surface tension γ_ρ, cf. Eq. (12), is consistently smaller for a gas bubble than for a liquid droplet. The surface tension of the planar vapour-liquid interface of the LJTS fluid at $T = 0.75$, which is $\gamma_\parallel = 0.493$ according to the correlation of Vrabec et al. [9], deviates relatively little from the γ_ρ values found for the droplet. The equimolar surface tension of bubbles from the present simulations, however, is significantly smaller than $\gamma_\parallel$.

On the basis of Hadwiger's theorem [61], it has been argued that the influence of geometry on the surface tension needs to be proportional to the mean curvature, the Gaussian curvature, or linear combinations thereof [62]. Such an interpretation of Hadwiger's theorem would explicitly rule out any curvature-independent effect. This cannot be upheld in the light of the present discussion, since the small-diameter effect, which has now been detected for bubbles as well as for droplets, exists analogously for planar slabs where curvature is strictly absent [35].

Beside the curvature and the diameter, further aspects of confinement may significantly influence vapour-liquid coexistence in small systems. In the past, such effects have largely been discussed separately from each other. A unified approach to describing the thermophysical properties of nanodispersed fluid phases would have to account for various size-dependent phenomena in a consistent way:

- The effect of curvature, cf. Tolman [47] and the present discussion.

- The effect of a small diameter, cf. Werth et al. [35] and the present discussion.

- The effect of the capillary wave cutoff, cf. Sengers and van Leeuwen [63]. The small circumference of the nano-dispersed phase imposes a restriction on the available modes, each of which contributes to the interfacial free energy.

- The effect of fluctuations, cf. Reguera et al. [56]. For a small dispersed phase, which is surrounded by a large bulk phase, the temperature, the density, and the volume can fluctuate significantly.

A theoretical approach which accounts for the interplay between these phenomena and yet retains the simplicity of Tolman's equation or the inverse cube law for the diameter effect is missing so far, however. Consequently, where no experimental data are available, molecular simulation is at present the only viable method for predicting the properties of nano-dispersed phases.

6. Conclusion

Molecular simulation is feasible up to the micrometre length scale by massively-parallel molecular dynamics today, facilitating an analysis of the size dependence for interfacial phenomena which it would otherwise be relatively hard to investigate in a reliable way. By molecular simulation, which is firmly founded on statistical mechanics, such effects can be rigorously investigated. In combination with the previous research of Malijevsky and Jackson [27] on droplets as well as Werth et al. [35] on thin slabs, present results on gas bubbles complete the recent body of work on the interplay of distinct effects

due to a high curvature of the interface and a small diameter of the dispersed phase, respectively.

Regarding the thermodynamic properties of nano-dispersed fluid phases, Tröster and Binder [25] have recently pointed out that as for small droplets there is, for instance, a significant deviation from the planar surface tension, but this effect does not consistently agree with the Tolman equation, 'neither the capillarity approximation nor the Tolman parametrization [...] should be employed in any serious quantitative work.' The present analysis supports this conclusion. Instead of the Tolman equation, a new theoretical framework needs to be developed to describe the various size-dependent effects related to the curvature, the diameter, and possibly the circumference as well as the volume, which controls the magnitude of fluctuations, in a coherent way.

Acknowledgment. The authors would like to thank BMBF for funding the SkaSim project, DFG for funding the Collaborative Research Centre MICOS (SFB 926), Akshay Bedhotiya for carrying out some of the molecular simulations of gas bubbles, Sebastian Eichelbaum and Mario Hlawitschka as well as Gerik Scheuermann for employing one of the present gas bubbles as a test case for PointAO shading, Kai Sundmacher for his encouragement, and Jadran Vrabec for his continuous support, as well as Stefan Becker, Ruslan Davidchack, Sergey Lishchuk, Andrew Masters, Erich Müller, and Stephan Werth for fruitful discussions. The present work was conducted unter the auspices of the Boltzmann-Zuse Society of Computational Molecular Engineering (BZS), and the MD simulations were carried out on the *elwetritsch* cluster, Regionales Hochschulrechenzentrum Kaiserslautern, within the scientific computing project TUKL-MSWS.

References

[1] J. W. Gibbs, Transact. Connecticut Acad. Arts Sci. 3 (1878) 108–248, 343–524.

[2] W. G. Chapman, K. E. Gubbins, G. Jackson, M. Radosz, Ind. Eng. Chem. Res. 29 (1990) 1709–1721.

[3] A. Müller, J. Winkelmann, J. Fischer, AIChE J. 42 (1996) 1116–1126.

[4] J. Gross, G. Sadowski, Ind. Eng. Chem. Res. 40 (2001) 1244–1260.

[5] R. W. Zwanzig, J. Chem. Phys. 22 (1954) 1420–1426.

[6] M. S. Wertheim, J. Stat. Phys. 35 (1984) 19–34.

[7] J. E. Mayer, J. Chem. Phys. 5 (1937) 67–73. 3177–3184.

[8] A. I. Rusanov, E. N. Brodskaya, J. Colloid Interface Sci. 62 (1977) 542–555.

[9] J. Vrabec, G. K. Kedia, G. Fuchs, H. Hasse, Molec. Phys. 104 (2006) 1509–1527.

[10] I. Napari, J. Julin, H. Vehkamäki, J. Chem. Phys. 131 (2009) 244511.

[11] M. Horsch, J. Vrabec, J. Chem. Phys. 131 (2009) 184104.

[12] N. Lümmen, B. Kvamme, J. Phys. Chem. B 112 (2008) 12374–12385, 15262.

[13] Y. Gan, V. P. Carey, Int. J. Heat Mass Transfer 53 (2010) 2169–2182.

[14] I. Napari, H. Vehkamäki, K. Laasonen, J. Chem. Phys. 120 (2004) 165–169.

[15] Y. Nakamura, A. Carlson, G. Amberg, J. Shiomi, Phys. Rev. E 88 (2013) 033010.

[16] B. Hafskjold, T. Ikeshoji, Molec. Sim. 16 (1996) 139–150.

[17] G. Guevara Carrión, H. Hasse, J. Vrabec, in: B. Kirchner, J. Vrabec (Eds.), Multiscale Molecular Methods in Applied Chemistry, Springer, Heidelberg, 2012, pp. 201–249.

[18] P. Schapotschnikow, R. Pool, T. J. H. Vlugt, Molec. Phys. 105 (2007) 3177–3184, 106 (2008) 963–964.

[19] W. Eckhardt, A. Heinecke, R. Bader, M. Brehm, N. Hammer, H. Huber, H.-G. Kleinhenz, J. Vrabec, H. Hasse, M. Horsch, M. Bernreuther, C. W. Glass, C. Niethammer, A. Bode, H.-J. Bungartz, in: J. M. Kunkel, T. Ludwig, H. W. Meuer (Eds.), Supercomputing, Springer, Heidelberg, 2013, pp. 1–12.

[20] M. Schrader, P. Virnau, D. Winter, T. Zykova-Timan, K. Binder, Eur. Phys. J. Spec. Top. 177 (2009) 103–127.

[21] J. Vrabec, M. Horsch, H. Hasse, ASME J. Heat Transfer 131 (2009) 043202.

[22] B. J. Block, S. K. Das, M. Oettel, P. Virnau, K. Binder, J. Chem. Phys. 133 (2010) 154702.

[23] J. G. Sampayo Hernández, A. Malijevský, jr., E. A. Müller, E. de Miguel, G. Jackson, J. Chem. Phys. 132 (2010) 141101.

[24] S. K. Das, K. Binder, Phys. Rev. Lett. 107 (2011) 235702.

[25] A. Tröster, K. Binder, Phys. Rev. Lett. 107 (2011) 265701.

[26] M. Horsch, H. Hasse, A. K. Shchekin, A. Agarwal, S. Eckelsbach, J. Vrabec, E. A. Müller, G. Jackson, Phys. Rev. E 85 (2012) 031605.

[27] A. Malijevský, jr., G. Jackson, J. Phys.: Cond. Mat. 24 (2012) 464121.

[28] T. L. Hill, Thermodynamics of Small Systems, W. A. Benjamin, New York, 1964.

[29] D. Kashchiev, Nucleation: Basic Theory with Applications, Butterworth-Heinemann, Oxford, 2000.

[30] J. S. Rowlinson, B. Widom, Molecular Theory of Capillarity, Clarendon, Oxford, 1982.

[31] H. Vehkamäki, Classical Nucleation Theory in Multicomponent Systems, Springer, Heidelberg, 2006.

[32] E. de Miguel, J. Phys. Chem. B 112 (2008) 4674–4679.

[33] K. Binder, Phys. Rev. A 25 (1982) 1699–1709.

[34] M. P. Gelfand, M. E. Fisher, Phys. A 166 (1990) 1–74.

[35] S. Werth, S. V. Lishchuk, M. Horsch, H. Hasse, Phys. A 392 (2013) 2359–2367.

[36] E. Salomons, M. Mareschal, J. Phys.: Cond. Mat. 3 (1991) 3645–3661.

[37] J. P. R. B. Walton, D. J. Tildesley, J. S. Rowlinson, J. R. Henderson, Molec. Phys. 48 (1983) 1357–1368.

[38] P. G. Debenedetti, Metastable Liquids: Concepts and Principles, Princeton University Press, 1996.

[39] J. Vrabec, H. Hasse, Molec. Phys. 100 (2002) 3375–3383.

[40] A. I. Rusanov, D. V. Tatyanenko, A. K. Shchekin, Colloid J. 72 (2010) 673–678.

[41] S. M. Thompson, K. E. Gubbins, J. P. R. B. Walton, R. A. R. Chantry, J. S. Rowlinson, J. Chem. Phys. 81 (1984) 530–542.

[42] J. K. Percus, L. A. Pozhar, K. E. Gubbins, Phys. Rev. E 51 (1995) 261–265.

[43] M. Born, K. Fuchs, Proc. R. Soc. London A 166 (1938) 391–414.

[44] A. Dillmann, G. E. A. Meier, J. Chem. Phys. 94 (5) (1990) 3872–3884.

[45] A. Laaksonen, I. J. Ford, M. Kulmala, Phys. Rev. E 49 (6) (1994) 5517–5524.

[46] R. C. Tolman, J. Chem. Phys. 16 (1948) 758–774.

[47] R. C. Tolman, J. Chem. Phys. 17 (1949) 333–337.

[48] M. J. P. Nijmeijer, C. Bruin, A. B. van Woerkom, A. F. Bakker, J. M. J. van Leeuwen, J. Chem. Phys. 96 (1991) 565–576.

[49] T. Frolov, Y. Mishin, J. Chem. Phys. 131 (2009) 054702.

[50] A. E. van Giessen, E. M. Blokhuis, J. Chem. Phys. 131 (2009) 164705.

[51] B. B. Laird, R. Davidchack, J. Chem. Phys. 132 (2010) 204101.

[52] C. Niethammer, M. Horsch, S. Becker, M. Bernreuther, M. Buchholz, W. Eckhardt, A. Heinecke, S. Werth, H.-J. Bungartz, C. W. Glass, H. Hasse, J. Vrabec (2013) In preparation.

[53] J. Janeček, J. Phys. Chem. B 110 (2006) 6264–6269.

[54] R. Yokota, L. A. Barba, Int. J. HPC Applicat. 26 (2012) 337–346.

[55] M. P. A. Fisher, M. Wortis, Phys. Rev. B 29 (1984) 6252–6260.

[56] D. Reguera, R. K. Bowles, Y. Djikaev, H. Reiss, J. Chem. Phys. 118 (2003) 340–353.

[57] S. Eichelbaum, G. Scheuermann, M. Hlawitschka, in: M. Hlawitschka, T. Weinkauf (Eds.), Proc. EuroVis 2013, Eurographics, 2013, p. 148 (SP).

[58] M. T. Horsch, S. K. Miroshnichenko, J. Vrabec, C. W. Glass, C. Niethammer, M. F. Bernreuther, E. A. Müller, G. Jackson, in: C. Bischof, H.-G. Hegering, W. E. Nagel, G. Wittum (Eds.), Competence in High Performance Computing, Springer, Heidelberg, 2012, pp. 73–84.

[59] B. Widom, J. Chem. Phys. 86 (1982) 869–872.

[60] M. Horsch, S. Becker, J. M. Castillo Sánchez, S. Deublein, A. Fröscher, S. Reiser, S. Werth, J. Vrabec, H. Hasse (2013) To appear, arXiv:1305.4048 [cond–mat.soft].

[61] H. Hadwiger, Vorlesungen über Inhalt, Oberfläche und Isoperimetrie, Springer, Berlin, 1957.

[62] P.-M. König, R. Roth, K. R. Mecke, Phys. Rev. Lett. 93 (2004) 160601.

[63] J. V. Sengers, J. M. J. van Leeuwen, Phys. Rev. A 39 (1989) 6346–6355.

Table 1:

N	V	$\rho'_{\max}$	ρ'_∞	ρ''_0	$p'(\rho'_\infty)$	$p''(\rho'_\infty)$	$-R_\rho$	$-R_\kappa$	
7 303	10 648	0.7348(4)	0.736(2)	0.023(3)	−0.16	0.0061	5.6	6.1	
9 551	13 824	0.7364(2)	0.7365(3)	0.0145(8)	−0.15	0.0061	5.9	6.2	
20 514	29 791	0.7426(7)	0.745(1)	0.02(1)	−0.101	0.0068	8.1	9.2	
18 107	27 000	0.747(2)	0.746(1)	0.008(3)	−0.093	0.0069	8.7	9.9	
42 474	64 000	0.7495(6)	0.7493(3)	0.010(1)	−0.068	0.0072	12.1	13.1	
34 944	54 872	0.7540(8)	0.751(3)	0.009(2)	−0.058	0.0074	12.6	15.1	[60]
75 794	117 649	0.7522(3)	0.7521(5)	0.011(1)	−0.048	0.0075	16.0	17.7	
122 232	195 112	0.7537(3)	0.7538(2)	0.0113(3)	−0.035	0.0077	20.0	23.0	
263 163	438 976	0.7557(2)	0.7556(4)	0.0117(5)	−0.022	0.0079	28.0	32.8	

Number of particles N and simulation volume V for a series of canonical ensemble MD simulations of LJTS bubbles in equilibrium (at $T = 0.75$). The maximal density $\rho'_{\max}$ of the liquid (in the outer region of the simulation volume) was extracted from the density profile. An extrapolated density ρ'_∞ of the liquid phase was also determined by following an approximation for the outer part of the the density profiles, cf. Eq. (21), to an infinite distance from the centre of the bubble. The gas density ρ''_0 was determined in a region closer than 1.5 to the centre of the bubble. (Errors for the density, with a magnitude corresponding to that of the final digit, are given in parentheses.) The thermodynamic liquid and vapour pressures $p'(\rho'_\infty)$ and $p''(\rho'_\infty)$ to be used within the Gibbs approach, respectively, were computed from the extrapolated liquid density by a fifth-order virial expansion [58];

they may deviate from the mechanical pressure. From the equimolar and capillarity radii R_ρ and R_κ, respectively, which are negative by the convention employed here, the excess equimolar radius $\eta = R_\rho - R_\kappa$ can be obtained; the value of η is found to be positive (and of the order of 1 σ).

Table 2:

N	V	R_ρ	μ	$p'(\Delta\mu)$	
18 107	27 000	− 8.7	−3.55(3)	−0.13(4)	
34 944	54 872	−12.6	−3.51(2)	−0.10(3)	[60]
N	V	s_ρ	μ_{sat}	p_{sat}	
7 079	18 341	8.5	−3.37(2)	0.0084	[60]
10 409	26 971	12.5	−3.37(2)	0.0084	
N	V	R_ρ	μ	$p'(\Delta\mu)$	
2 425	27 000	8.6	−3.28(6)	0.08(6)	
6 844	54 872	12.4	−3.31(4)	0.05(5)	[60]

Results for bubbles (top), planar slabs (middle), and droplets (bottom) from equilibrium MD simulation of the LJTS fluid in the canonical ensemble with N particles and a simulation volume of V at a temperature of $T = 0.75$, where the equimolar radii R_ρ and slab thicknesses s_ρ were determined from density profiles, while the chemical potential μ was computed by Widom's test particle method [59]. The liquid pressure p' was calculated from the deviation $\Delta\mu$ between the chemical potential at the planar and curved interfaces on the basis of an equation of state [58]. The error for μ and p', respectively, is indicated in parentheses, where the error of is of the same magnitude as the last given digit.

Table 3:

N	V	$p' - p''$	$1/R_\rho$	γ_ρ
7 303	10 648	−0.16(1)	−0.180	0.45(4)
9 551	13 824	−0.159(5)	−0.169	0.47(2)
20 514	29 791	−0.11(1)	−0.123	0.44(4)
18 107	27 000	−0.10(1)	−0.115	0.43(4)
42 474	64 000	−0.075(6)	−0.0827	0.46(3)
75 794	117 649	−0.056(7)	−0.0626	0.44(5)
122 232	195 112	−0.043(4)	−0.0500	0.43(4)
N	V	$p' - p''$	$1/R_\rho$	γ_ρ
15 237	166 375	0.060(2)	0.0626	0.48(2)
12 651	140 608	0.065(2)	0.0668	0.49(2)
10 241	110 592	0.070(1)	0.0716	0.49(1)
6 619	74 088	0.080(2)	0.0831	0.48(1)
5 161	54 872	0.085(3)	0.0902	0.47(1)
3 762	39 304	0.102(2)	0.100	0.51(1)
1 418	21 952	0.15(1)	0.145	0.52(4)

Number of molecules N, simulation volume V, pressure difference $p' - p''$ between the coexisting fluid phases, equimolar curvature $1/R_\rho$, and equimolar surface tension γ_ρ, cf. Eq. (12), from the present MD simulations of gas bubbles (top) as well as the MD simulations of liquid droplets (bottom) from previous work [26], for the LJTS fluid at $T = 0.75$. Numbers in parentheses represent the error, with the magnitude corresponding to that of the last given digit (only results for γ_ρ with an error of 0.05 or less are shown here).

Figure 1:

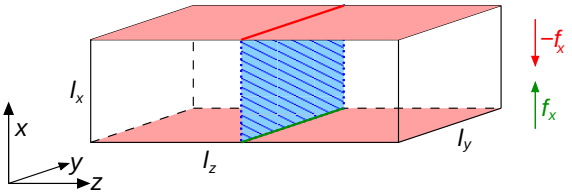

Diagram illustrating the mechanical definition of the surface tension. The two faces of the box with an orientation perpendicular to the x axis experience forces in opposite directions, expressing the tendency of an interface situated in the centre of the box to contract. The magnitude of the force f_x is proportional to the surface tension γ and the length of the contact line l_y.

Figure 2:

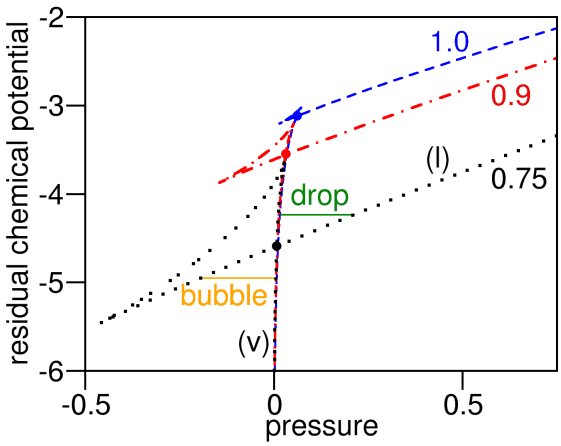

Isothermal dependence of the residual chemical potential $\mu_{\rm res}$, cf. Eq. (6), on the pressure p from a virial expansion [58] for the truncated-shifted Lennard-Jones potential at reduced temperatures of 0.75 ($\cdots$), 0.9 ($\cdot$ – $\cdot$), and 1.0 (– –). The plot extends over the whole range of vapour (v) and liquid (l) densities including stable, metastable and unstable states. Self-intersections of the isotherms (•) correspond to the phase equilibrium condition at a planar interface, i.e. $\mu' = \mu'' = \mu_{\rm sat}(T)$ and $p' = p'' = p_{\rm sat}(T)$. Solid horizontal lines: Vapour-liquid equilibrium at a curved interface characterized by the Laplace equation, cf. Eq. (5), where the reduced temperature is 0.75 and the pressure is smaller outside than for the dispersed phase, which is confined by the interface, with a pressure difference of $p' - p'' = \pm\ 0.2$ in reduced units.

Figure 3:

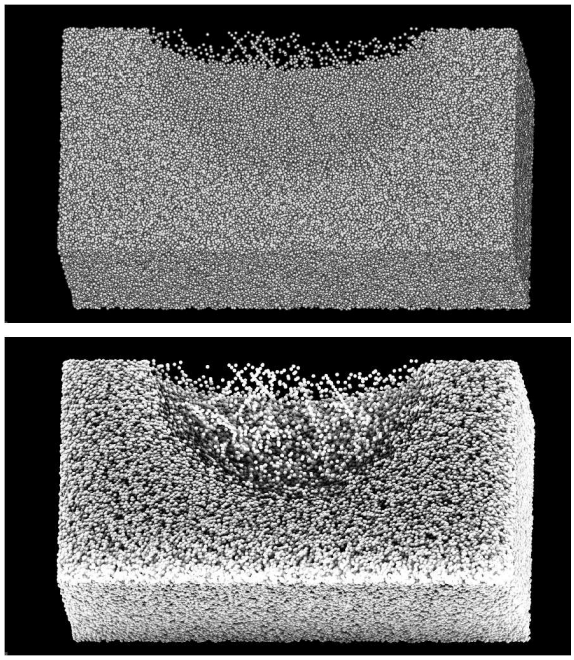

Visualization of the same configuration by Phong shading (top) as opposed to the novel PointAO shading algorithm (bottom), cf. Eichelbaum et al. [57].

Figure 4:

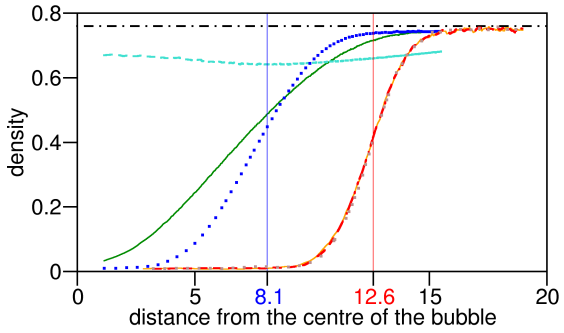

Density profiles of LJTS bubbles surrounded by liquid, collected during different sampling intervals from two MD simulation runs, both in the canonical ensemble at $T = 0.75$. The density profiles on the right side correspond to samlpling intervals from 45 000 to 60 000 (—), 60 000 to 70 000 (– –), and 70 000 to 80 000 time steps (· · ·) after simulation onset, with $N = 34\ 944$ and $V = 38 \times 38 \times 38$, exhibiting fast convergence and negligible fluctuations [60]. The density profiles on the left side, corresponding to $N = 20\ 514$ and $V = 31 \times 31 \times 31$ with sampling intervals from 14 to 16 (—), 24 to 26 (– –), and 34 to 36 million time steps (· · ·) after simulation onset, alternate between configurations where a bubble is present and homogeneous subsaturated liquid configurations. Horizontal dash-dotted line: Density of the bulk liquid at saturation; Vertical lines: Equimolar radii of the bubbles.

Figure 5:

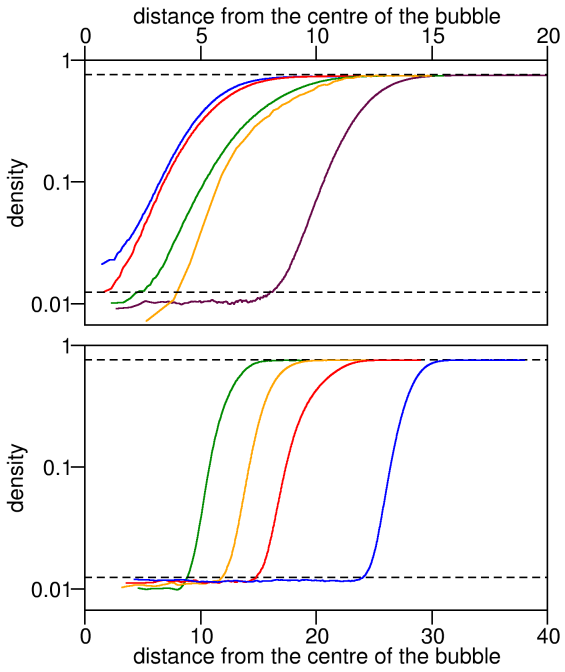

Density profiles of bubbles in equilibrium with a subsaturated liquid phase from MD simulation of the LJTS fluid in the canonical ensemble (—) in comparison with the vapour and liquid densities at saturation (– –), for a temperature of $T = 0.75$. Top: Results for five relatively small bubbles with equimolar radii $R_\rho = -5.6$, -5.9, -8.1, -8.7, and -12.1 (from left to right); Bottom: Results for four relatively large bubbles with $R_\rho = -12.6$, -16.0, -20.0, and -28.0 (from left to right), including simulation results for $R_\rho = -12.6$ from previous work [60].

Figure 6:

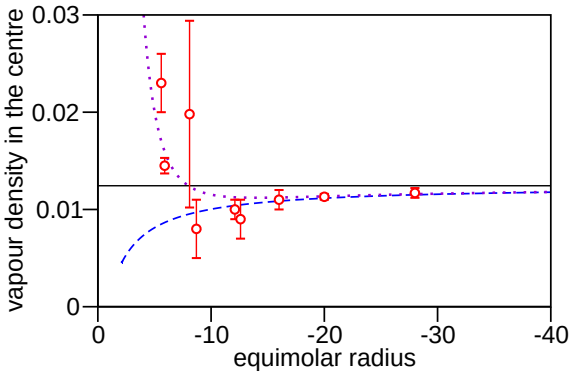

Density in the centre over the equimolar radius of gas bubbles, which is negative here by convention, from present MD simulations of the LJTS fluid in the canonical ensemble at $T = 0.75$ ($\circ$), including a data point for $R_\rho = -12.6$ from previous work [60], in comparison with the vapour density at saturation (—) and a thermodynamic prediction from the capillarity approximation (– –), considering curvature effects only and assuming $\gamma = \gamma_\parallel$ (and hence $R = R_\kappa = R_\rho$), as well as a correlation which also includes a deviation from the capillarity approximation proportional to the inverse cube of the radius ($\cdots$), i.e. $\Delta\rho = -1.5/R_\rho^{-3}$, due to the small-diameter effect found by Malijevský and Jackson [27].

Figure 7:

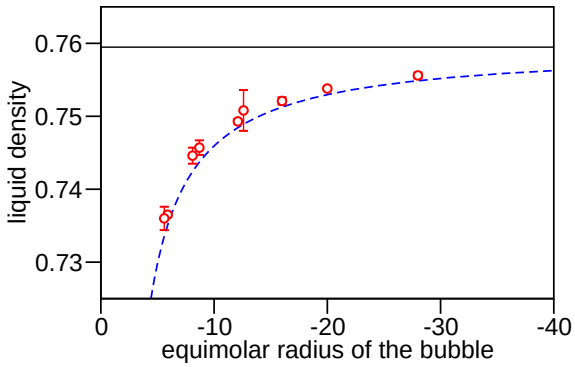

Liquid density ρ'_∞, obtained by extrapolating the density profiles from present MD simulations to an infinite distance from the centre of the gas bubble ($\circ$), over the equimolar radius R_ρ, which is negative by the convention employed here, for the LJTS fluid in the canonical ensemble at $T = 0.75$, including a data point for $R_\rho = -12.6$ from previous work [60], in comparison with the liquid density at saturation (—) as well as a thermodynamic prediction from the capillarity approximation (– –), considering curvature effects only and assuming $\gamma = \gamma_\parallel$ (and hence $R = R_\kappa = R_\rho$).